WRN Exonuclease Structure, Molecular Mechanism, and DNA End Processing Role

J. Jefferson P. Perry[1,2], Steven M. Yannone[2,†], Lauren G. Holden[1], Chiharu Hitomi[1], Aroumougame Asaithamby[4], Seungil Han[2,3], Priscilla K. Cooper[2], David J. Chen[4] & John A. Tainer[1,2,†]

[1] Department of Molecular Biology and Skaggs Institute for Chemical Biology. The Scripps Research Institute, La Jolla, California, 92037.

[2] Life Sciences Division, Department of Molecular Biology, Lawrence Berkeley National Laboratory, Berkeley, California, 94720.

[3] Pfizer Global Research and Development, Exploratory Medicinal Sciences (EMS), MS4039 Eastern Point Road, Groton, CT 06340.

[4] Division of Molecular Radiation Biology, Department of Radiation Oncology, UT Southwestern Medical Center, Dallas, TX 75390-9187.

[†] Correspondence should be addressed to JAT or SMY

ABSTRACT

WRN is unique among the five human RecQ DNA helicases by having a functional exonuclease domain (WRN-exo) and being defective in the premature aging and cancer-related disorder Werner syndrome. Here, we characterize WRN-exo crystal structures, biochemical activity and participation in DNA end-joining. Metal ion complex structures, active site mutations and activity assays reveal a two-metal-ion mediated nuclease mechanism. The DNA end-binding Ku70/80 complex specifically stimulates WRN-exo activity, and structure-based mutational inactivation of WRN-exo alters DNA end-joining in human cells. We furthermore establish structural and biochemical similarities of WRN-exo to DnaQ family replicative proofreading exonucleases, with WRN-specific adaptations consistent with dsDNA specificity and functionally important conformational changes. These results indicate WRN-exo is a human DnaQ family member and support analogous proof-reading activities that are stimulated by Ku70/80 with implications for WRN functions in age related pathologies and maintenance of genomic integrity.

Werner Syndrome (WS) is an autosomal recessive disorder that gives rise to multiple progeroid pathologies, including osteoporosis, atherosclerosis and a greatly increased cancer incidence[1]. Genomic instability is characteristic of WS cells, which show extensive chromosomal deletions, elevated rates of homologous recombination, prolonged S-phase DNA synthesis and defective telomere maintenance[2]. WS is caused by the loss of function of a single gene, *WRN*[3], which encodes a 1432 amino acid protein that contains a C-terminal nuclear localization signal. The biological functions of WRN protein remain incompletely defined. To date, all identified mutations in WS individuals have nonsense or frameshift mutations leading to a truncated protein that cannot localize to the nucleus[4,5] and is generally degraded in the cytoplasm[6,7].

WRN belongs to the RecQ helicase family, which is widely distributed across the three domains of life and named after the first member discovered in *E. coli*[8]. The human genome contains five RecQ genes, *RecQ1, BLM, WRN, RecQ4L* and *RecQ5*. Mutations in *BLM* and *RecQ4L* cause Bloom Syndrome (BS) and Rothmund-Thomson syndrome (RTS) respectively[8]. WS, BS and RTS share a predisposition to cancer, but significant pathological differences suggest that each disease pathway is functionally distinct. Biochemical characterization of the human RecQ helicases has shown ATPase activity and unwinding of partial duplex DNA substrates with 3′-5′ polarity. Alternate DNA conformations are preferred over dsDNA, suggesting roles for human RecQ helicases in replication, recombination and repair events[8].

WRN is unique among all RecQ helicases in having an N-terminal 3′-5′ exonuclease domain first identified by sensitive sequence alignment methods[9,10]. Subsequently, recombinant WRN protein was shown to exhibit 3′-5′ exonuclease

activity on dsDNA with 3′ recessed termini[11]. WRN-exonuclease functions on a variety of structured DNA substrates including bubbles, stem-loops, forks and Holliday junctions, as well as RNA-DNA duplexes, implicating roles for WRN in DNA replication, recombination and repair[12]. WRN 3′-5′ helicase activity exhibits substrate specificity similar to that for the exonuclease, suggesting that the two WRN enzymatic activities may have coordinated functions on several classes of DNA structures[2,13].

Cultured WS cells are hypersensitive to certain DNA damaging agents, including camptothecin, 4-nitroquinoline-1-oxide, interstrand crosslinkers, and display a mild, yet distinct sensitivity to ionizing radiation[14,15,16]. One particularly toxic class of DNA lesion arising from exposure to these agents is the DNA double-strand break (DSB). Human somatic cells repair DSBs via the error-free homologous recombination (HR) or the more predominant, but error-prone, non-homologous end-joining (NHEJ) pathway. WRN function in HR has been implicated in part by interactions with the Mre11-Rad50-NBS1 complex[15], Rad52[17] and colocalization with Rad51 in camptothecin-treated cells[18]. Similarly, a link to the NHEJ pathway was initially indicated by the stimulation of WRN exonuclease activity by the DNA-PK components Ku70/80[19,20]. More recent studies revealed that WRN activity is regulated by *holo*-DNA-PK and that WRN is an *in vivo* substrate of DNA-PK, suggesting physiological and functional interactions[16,21-24]. Further support for functional WRN-Ku70/80 interactions comes from the characterization of an endogenous complex containing WRN, Ku70/80 and poly(ADP-ribose) polymerase (PARP-1)[25]. PARP-1 binds DNA at sites of single- and double-strand breaks, and is implicated to function in the control of genomic integrity and mammalian life span. Despite the enigmatic nature of precise WRN molecular functions,

WRN interactions with key DNA repair proteins suggest a coordinated function of WRN with DNA repair processes in human cells.

Here, we report five crystallographic structural determinations of the human WRN exonuclease domain (WRN-exo) up to 2.0 Å resolution. Our metal ion WRN-exo structural complexes, mutational inactivation of key active site residues and activity assays reveal a high degree of structural and mechanistic conservation with a family of replicative proofreading exonucleases. However, the low sequence identities shared between WRN-exo and its closest structural homolog, the Klenow fragment exonuclease (KF-exo), explains the significant divergence in function. We observe that Ku70/80 stimulates WRN-exo catalytic activity but inhibits KF-exo, suggesting that the WRN-exo domain may help impart WRN-Ku70/80 mediated functions. Additionally, we observe an *in vivo* requirement for WRN exonuclease activity, whereby inactivation alters plasmid DNA end-joining in a manner similar to that seen with cells completely lacking WRN protein.

RESULTS

WRN-exo Domain Crystallization

We first expressed and purified a recombinant WRN N-terminal construct, WRN_{1-333}, known to exhibit exonuclease activity[11]. To define the boundaries of the minimal exonuclease domain within this construct, WRN_{1-333} was subjected to limited proteolysis with either trypsin or chymotrypsin. Tandem mass spectrometry and N-terminal sequencing then delineated the degradation products. These data revealed a protease resistant core exonuclease domain containing residues 38-236 (data not shown).

Recombinant WRN_{38-236} expressed from *E. coli* is monomeric with an estimated mass of 25 KDa, as judged by dynamic light scattering and gel filtration chromatography. We obtained WRN-exo protein crystals through vapor diffusion crystallization experiments, and these crystals diffracted up to 2.0 Å resolution with synchrotron radiation. Multiple-wavelength anomalous diffraction (MAD) phasing experiments on a selenomethionine substituted WRN-exo protein crystal produced an interpretable electron density map (Fig. 1, Table 1). The crystals belonged to space group $P3_221$, and the asymmetric unit contains one molecule. The last two histidines of the N-terminal hexa-histidine tag and residues 38-230 are clearly visible in the electron density maps, with only the C-terminal six residues of the molecule being disordered.

Structural Conservation with the DnaQ Family of Proteins

The WRN-exo domain has an α–β fold that consists of a central β-sheet (strands β1-β6) surrounded by 7 α-helices, (α1-α7), two 3_{10} helices (3_{10}1 and 3_{10}2) and a small, two-stranded sheet (β0 and β1)(Fig. 2a). The strands of the central β-sheet are parallel, with the exception of β3, and the sheet is surrounded by helices α1-3 & 3_{10}2 on one face and α4-7 and 3_{10}1 on the other. Our analysis of the WRN-exo fold using the Dali server showed structural homology to the DnaQ family of 3′-5′ exonucleases. WRN-exo is to our knowledge the first human structural domain determined for the DnaQ family. The well-conserved WRN-exo active site is contained within a large cavity on one face of the molecule. This cavity is built from helices α3-7 with the edge of strand β2 at the base. Residues D82 and E84, from β-2, and D143 and D216 from α-3 and α-7, respectively, form the catalytic core (Fig. 2a, e).

The DnaQ structural family contains 3′-5′ exonuclease domains from archaea, bacteria and viruses (SCOP database). Among the DnaQ family members, *E. coli* DNA I polymerase 3′-5′ proofreading exonuclease domain (Klenow Fragment, KF) shares the highest degree of structural conservation with WRN-exo[26]. Using SEQUIOA[27], the WRN-exo and KF exonuclease (KF-exo) structures overlay with a rmsd of 2.09 $Å^2$ for the Cα atoms of 144 structurally equivalent residues. Despite this high degree of architectural conservation, the sequences of these two proteins are significantly divergent and share only 16% identity (Fig. 2e). However, the key active site residues are conserved and structural superimposition reveals conservation of both the active site architecture and the core secondary structural elements (Fig. 2b, d). The smaller β-0 and β-1 of the small external sheet and two 3_{10} helices are secondary structural elements specific to WRN (Fig. 2 b and e). There is also significant sequence and structural variation evident in the connecting loop regions. Most notably, the two loops proximal to the active site are variant. The β2-β3 loop in WRN has an extra two amino acids and altered conformation, and two 3_{10} helices and five loop residues between helices α6-α7 are absent in WRN.

The DnaQ family contains one other eukaryotic member, the *A. thaliana* protein 'At5G06450' (pdb code: 1VK0). The *A. thaliana* protein crystal structure was determined by structural genomics studies and its function remains unknown. We found that the *A. thaliana* protein structure superimposes onto WRN-exo with an rmsd of 2.22 $Å^2$ for 146 structurally equivalent residues and 14% sequence identity (Fig. 2c,e). The *A. thaliana* homolog has helix α6 in the position of WRN β7 and the *A. thaliana* β0 strand stacks at the end of the central sheet. The β2-β3 loop in WRN and the *A. thaliana* protein are

both extended when compared to KF-exo and share an equivalent number of residues, though all residues are clearly refined in the WRN structure. The α6-α7 loop region of the *A. thaliana* homolog is truncated by seven amino acids compared with WRN. Additionally, the active site for this *A. thaliana* protein differs from WRN-exo and KF-exo: a tyrosine replaces WRN E84, alanine replaces WRN Y212 and a glutamate replaces WRN D216 (fig 2d). This indicates that bacterial KF-exo may be more closely related to WRN-exo than the *A. thaliana* protein.

Active Site Metals

To further characterize the WRN-exo molecular mechanism and metal ion dependence, we determined crystal structures of WRN-exo complexes with Mg^{2+} ions [2.2 Å resolution], Mn^{2+} ions [2.4 Å resolution], or Mn^{2+} ions and dGMP [2.0 Å resolution] (table 1). In the presence of either Mn^{2+} or Mg^{2+} ions, WRN-exo exhibits 3′-5′ nuclease activity on dsDNA substrates with five-base 5′-overhangs (Fig. 3a). Exonuclease activity is increased in the presence of Mn^{2+} relative to Mg^{2+}, and the substrate degradation pattern with equimolar amounts of Mn^{2+} and Mg^{2+} is indistinguishable from Mn^{2+} alone (Fig. 3a). Therefore, Mn^{2+} supports a higher catalytic activity in these *in vitro* assays even though Mg^{2+} is the more likely co-factor in the cell. In both the Mn^{2+} and Mg^{2+} crystal soaks, two metal ions are accommodated into the active site without altering the WRN-exo structure. The Mn^{2+} ions were refined at 100% occupancy, with B values of 31.4 and 42.8 $Å^2$ for site M_A and site M_B, respectively, for the 2.0 Å dataset. The Mg^{2+} ions were refined at 100% and 50% occupancy with B values of 57.0 and 45.6 $Å^2$ for sites M_A and M_B, respectively. The Mn^{2+} or Mg^{2+} metal ions bind in a similar manner

with the distance separating the metal ions at sites M_A and M_B being 3.7 Å. Coordination of metal ions is most clearly observed in the higher resolution Mn dataset: The inner metal ion, M_A, has approximate octahedral geometry and is directly coordinated by D82, E84, and D216. The outer metal ion, M_B, also has approximate octahedral geometry and directly ligates one side chain, D82, which bridges the two metal ions. D143, conserved within the superfamily, has an indirect interaction with the M_B metal ion via two water molecules (Fig. 3b). The correct ligation of these metal ions is essential for WRN-exo activity, as a structure-based E84A mutation completely perturbs exonuclease function in our nuclease assays (see Fig 5a). Overall, the active site structures of WRN-exo metal ion complexes when compared to other family members are remarkably similar, despite significant divergence in sequence identity, substrate specificity and relative activities.

Lanthanide (III) ions are well accommodated into protein metal binding sites and can cause a potent inhibition of enzymatic activities[28]. We found that the lanthanide europium does not support WRN-exo activity, and inhibits Mg^{2+} or Mn^{2+} based activity in our exonuclease enzymatic assays (Fig. 3a). We therefore determined a 2.0 Å resolution structure of a WRN-exo Eu^{3+} metal ion complex (Table 1) to define any structural changes that may account for loss of activity. Similar to the Mg^{2+} and Mn^{2+} ions, the active site of WRN-exo accommodates two Eu^{3+} ions (Fig. 3c, d), at positions M_A and M_B. This is distinct from the KF-exo structures that bind only one Eu^{3+} ion, typically in the M_A position[28]. The two europium ion sites in WRN-exo are somewhat disordered/poorly occupied and were refined with occupancies of 70 and 50% and B values of 58.1 and 54.3 $Å^2$ for site M_A and site M_B, respectively. The binding of Eu^{3+} ions

does not cause major alterations to the active site side chains, and therefore changes in protein structure are not likely to account for the inhibition of nuclease activity by europium. Instead, the Eu^{3+} M_A and M_B metal ions have moved slightly closer together, at 3.4 Å apart, and have slightly increased side chain ligation distance compared to the Mg^{2+} and Mn^{2+} complexes (Fig. 3c, d). Therefore, the inhibition observed for Eu^{3+} is possibly due to the altered charge state, and/or larger radii of bound Eu^{3+} ions causing misalignment of the scissile phosphate of the DNA substrate. In keeping with this hypothesis, studies with KF-exo have shown that movement of the scissile bond by 0.6 Å from its native position significantly reduces the initial velocity of the enzyme[29].

WRN-exo Substrate Binding Site

There are significant differences between the WRN-exo and the KF-exo nucleotide-binding region, including notable differences in surface electrostatics (Fig. 4a, b). WRN Y212, which is well conserved in the family and is critical in directing water-mediated attack of the phosphodiester bond, is oriented away from the active site (Fig. 4c). All the higher resolution KF-exo structures have substrate analogs or base products bound in the active site, but similar inactive tyrosine conformations have been observed in several other DNA polymerase structures in the absence of bound substrate[30-32]. The hydroxyl group of Y212 is vital to the WRN-exo active site mechanism, as a Y212F substitution significantly reduces but does not eliminate WRN-exo activity (Fig 5a). This suggests that the Y212 side chain reorients into the active site upon substrate binding.

Unlike KF-exo, the WRN R196 side chain on α-helix 6, which is adjacent to Y212, fits into the active site and forms a hydrogen bond to the metal binding residue

D216 (Fig. 4c). Modeling DNA substrates from KF-exo into the WRN active site indicates that R196 may also form interactions with the terminal phosphate group (Fig. 4d). The terminal ribose group would be expected to stack against W85 and the base should stack against C197 (Fig. 4d). Stacking on the opposing side of the terminal base is a leucine side chain in KF-exo, L361. However, the equivalent residue in WRN, L88, has its Cα positioned 10 Å away with its side chain pointing into solution (Fig. 4c,d). WRN L88 and KF L361 reside in the flexible β2-β3 loop region. The WRN β2-β3 loop (residues 85-98) has a two amino acid insertion, and its 'open' conformation is likely stabilized by crystal packing interactions of loop residue R91. A structure-based L88A mutation has no significant effect on WRN-exo catalytic activity (Fig. 5a), indicating other residues in this substrate-binding loop may be important. WRN L94 side chain is in the correct orientation and within 5.5 Å to the KF-exo Leu, but it is not well conserved in WRN homologous sequences. Instead, modeling of bound substrate indicates other residues within the β2-β3 loop, including Y89 and K93, which are strictly conserved among the WRN homologues or the well conserved N90 and R91, may also play a role in substrate binding (Fig. 4e).

The WRN-exo domain contains two single nucleotide polymorphisms (SNPs) that alter the encoded amino acid. Both SNPs occur at positions away from the active site but may alter enzyme stability and reside close enough to affect substrate binding. In the helicase region of WRN, the infrequent polymorphism R834C has been demonstrated to inhibit helicase activity[33]. This study was based on WRN homology to the *E. coli* RecQ helicase core structure[34], which suggests that the R834C mutation would perturb coordination of the terminal ATP phosphate that is required for catalysis.

We observe that the two known WRN-exo polymorphisms that alter amino acids, V114I and T172P, do not directly alter exonuclease activity of this minimal domain (Fig. 5a). The V114I polymorphism occurs in the first residue of 3_{10}-2, and this side chain in our wild type structure is oriented into the hydrophobic core of the molecule. Thus, the isoleucine variant is likely to be accommodated into the core without disturbing the overall WRN-exo structure, although the extra methyl group could disturb packing and possibly decrease stability. The T172P polymorphism resides in the α4-α5 loop on the surface of the molecule and has been previously described to cause a small reduction in the enzymatic activities of full-length WRN protein[33]. Since the WRN-exo T172P activity is not significantly perturbed, alterations in WRN activity may be due to disruption of WRN exonuclease-helicase coordination and/or reduced stability or folding in the larger protein.

In Vitro and *In Vivo* exonuclease activity

Full-length WRN is reported to interact with *holo*-DNA-PK and the DNA-PK heterodimeric subunit Ku70/80, which binds WRN in both the N and C-terminal regions, stimulating WRN exonuclease activity[16,19-24]. Therefore, we investigated whether Ku70/80 nuclease stimulation is inherent to the minimal WRN-exo domain. As previously observed for full-length WRN, the WRN-exo was stimulated under similar reaction conditions by the addition of Ku70/80 (Fig 5b; Fig 7b). To determine if the stimulation is inherent to DnaQ exonucleases or is characteristic of 3′-5′ exonucleases in general, we evaluated the influence of Ku70/80 on the structurally conserved KF-exo and the unrelated bacterial exonuclease III (Fig. 5b). In contrast to WRN-exo, KF-exo

nuclease activity was inhibited, while exonuclease III was unperturbed at lower concentrations and mildly inhibited at higher concentrations (Fig 5b). Substantially higher concentrations of Ku70/80 can inhibit all three nucleases almost completely (data not shown). Stimulation of WRN-exo by Ku70/80 was observed with either Mg^{2+} or Mn^{2+} metal cofactors (shown for Mg^{2+}). Increased WRN-exo activity occurs by the two metal ion-mediated mechanism, since the E84A control is catalytically inactive irrespective of Ku70/80 addition and Ku70/80 stimulates the minimal activity of Y212F, while the surface exposed T172P polymorphism exhibits stimulation comparable to wild type (data not shown). Additionally, a comparison of WRN-exo nuclease to full-length WRN revealed similar digestion patterns. (Fig 5b, right). However, full-length WRN appears to have higher specific activity, as the nearly equivalent levels of activity require six fold higher molar concentrations of WRN-exo than full-length protein. Taken together, the data suggest that the WRN-exo domain is comparable to the full-length protein in degrading dsDNA and in being specifically stimulated by Ku70/80 and that WRN-Ku mediated functions are inherent, at least in part, to the minimal nuclease domain.

The WRN-exonuclease activity has been implicated in DSB repair,[16,24,35] but it is not critical for lagging-strand DNA synthesis or for recombination at telomeres, where WRN helicase activity plays a role[36,37]. Therefore, we employed a previously established end-joining assay to determine if WRN-exo activity influences DNA end-joining in human cells. Linear blunt-ended plasmid DNA containing terminal direct repeats of 6 base pairs was transfected into cultured cells and recovered after 48 hours. Repair processes involving the microhomology at the ends of the plasmid to facilitate rejoining create a BstXI restriction site at the junction, while all other repair processes

do not[38] (Fig 6a). The relative use of microhomology for repair is determined by BstXI restriction of the amplified junction, with increased microhomology-mediated joining indicated by an increase in the proportion of PCR product cleaved by BstXI. Studies using this assay have determined that microhomology-mediated repair is significantly elevated in cells lacking NHEJ proteins ligase IV, XRCC4, Ku80 or DNA-Pkcs[39], but not in cells compromised for homologous recombination[40]. As expected, we find significantly elevated microhomology use in rodent cells lacking DNA-Pkcs (60%) relative to control rodent cells (10%)(Fig. 6b). WS cells also show this elevated microhomology use (81%) relative to both wild type human fibroblasts (9%) and WS cells complemented with WRN cDNA (8%)(Fig. 6c). Notably, the exonuclease-inactive E84A mutant WRN fails to fully complement the defect in WS cells (52%). To further evaluate this phenotype and ensure sequence-independent results, we conducted assays with a second reporter plasmid harboring 10 base pairs of homologous terminal sequence. Microhomology-mediated repair was assessed in WS fibroblasts transfected either with expression vectors for wild type WRN, a nuclease inactive mutant E84A, a helicase inactive mutant K577A, the double mutant, or the empty vector as a control (Fig 6d). With the reporter plasmid having 10 base pair homology, human WS cells also show elevated microhomology-mediated repair (76%), which is greatly reduced by wild type WRN expression (16%). Both the exonuclease (E84A) and helicase (K577A) mutants showed partial complementation of the defect (48% and 47% joining by microhomology, respectively), while the double mutant failed to complement this phenotype (73%) when expressed at comparable levels as wt WRN (Fig 6e). Thus, despite some variation in the levels of percent microhomology use between the two

reporter plasmids, cDNA encoding mutant WRN defective in either exonuclease or helicase activities failed to complement the WS cells. Therefore, the non-enzymatic functions of WRN do not suffice to complement the altered DSB end-joining in WS cells, whereas the WRN exonuclease and helicase activities are both required.

DISCUSSION

Our structures of the WRN-exo reveal a striking similarity to DnaQ family proteins. Metal ion complex structures (Fig. 3, Table 1) furthermore suggest that WRN-exo degrades nucleotide substrates by a two metal-ion mediated mechanism, analogous to that first observed in KF-exo[26]. The metal-ion mechanism is supported by Mg^{2+} and Mn^{2+} (Fig. 3), and similar to other exonucleases, the addition of lanthanide ions readily inhibits the reaction[28] (Fig. 3). Mutation of the active site residues, well conserved in the DnaQ family, also eliminates or significantly reduces catalytic activity. However, the two polymorphisms in WRN-exo that alter amino acids were not noted to have a significant effect on core nuclease activity (Fig. 5), distinct from an activity-disabling WRN helicase polymorphism[33].

WRN-exonuclease activity is not required for telomere functions, but it has been reported to influence DNA repair events in conjunction with helicase activity and a non-enzymatic function[41]. Using a plasmid rejoining assay[39], we observe that WRN-exo activity is required to fully complement a WS DNA end-joining phenotype (Fig. 6). This *in vivo* data does not define a specific cellular pathway, but the elevated microhomology-mediated repair in WS cells is similar to that observed in essential NHEJ proteins[39]. The mild radiation sensitivity of WS cells rules out WRN as an

essential DSB repair protein, but WRN-exo may still be utilized for resolution of a limited class of DSB substrates. Recent studies revealed that WRN accumulates at the sites of DSBs, but not at single-strand breaks or sites of oxidative damage[42], and that the WRN exonuclease activity alone can promote cellular survival after exposure to the DNA damaging agent *cis*-Pt[43,44]. Moreover, NHEJ-mediated repair products in WS cells exhibit extensive deletions relative to products from wild type cells, possibly indicating the substitution of WRN function by more processive or unregulated nucleases[35].

Interactions of Ku70/80 and PARP-1 with full-length WRN alter WRN-exo activity [16,19-24]. We discovered that equivalent Ku70/80/DNA molar ratios are able to stimulate the minimal WRN-exo domain but inhibit the structurally conserved KF-exo and do not perturb the activity of the bacterial exonuclease III, except at higher concentrations (Fig 5b). Thus, the exonuclease stimulation by Ku70/80 is not a generalized phenomenon common to all 3′-5′ exonucleases, or even those of the DnaQ family. Stimulation by Ku70/80 may result from several possible mechanisms, including alteration of DNA ends[8,12] or stabilization of an active conformation of WRN-exo on DNA, requiring movements of the β2-β3 loop and residue Y212 (Fig. 7d). This type of "open and closed" nuclease regulation is observed in the equivalent loop in DNA polymerase editing nucleases[32] and analogous to that controlling DNA polymerase active site elongation events[45].

Full-length WRN forms multimers[46], which likely influence its substrate specificities as well as helicase and exonuclease activities. This multimerization suggests a basis for the observed six-fold higher activity of full-length WRN compared to the core exonuclease domain (Fig. 5b, right). WRN RecQ homologues also exist in

oligomeric forms, including the hexameric and/or tetrameric rings of human BLM[47]. Moreover, a construct similar to WRN-exo forms homo-hexamers upon interaction with DNA or PCNA[46,48], and our WRN_{1-333} construct is multimeric[46]. Significantly, a WRN-exo hexameric ring model, which is based upon the *A. thaliana* (1VK0.pdb) structural homolog, has a central cavity containing the active site and positively charged surface (Fig. 4a), which is large enough to accommodate dsDNA substrate (Fig. 7a). Consistent with this model, we observed that WRN-exo crystals soaked with 2-deoxyguanosine 5-monophosphate (dGMP) bound the nucleotide at W145, central to the modeled ring (Table 1, Fig. 7c). The W145A WRN-exo mutant retains activity but with evidently altered processivity, consistent with a possible DNA binding role (Fig. 7b). This ring model may indicate how WRN assemblies support activity on complex DNA structures, and it potentially accounts in part for the higher activity of the full-length protein relative to the WRN-exo (Fig. 5b). Interestingly, similar internal and external dimensions are shared for the WRN-exo hexamer (30 Å by 85 Å) and Ku70/80[49] (35 Å by 65 to 120 Å) rings (Fig. 7d). Our model thus suggests a possible regulatory mechanism that would involve at least transient stacking of the Ku70/80 and WRN-exo rings on DNA ends. This ring-stacking model would allow efficient protein hand offs and regulation of DNA end processing, while avoiding the risks from possible release of broken DNA strands. Such reversible associations are a recurring theme among many DNA damage responsive proteins[50].

Taken together, the results presented here establish WRN-exo as a DnaQ family member that therefore reveals the conservation of this family from humans to bacteria and archaea. In *E. coli* the KF-exo DnaQ domain confers a proofreading nuclease

activity with limited processivity, to ensure the fidelity of DNA replication. Structural and biochemical similarities shared by WRN-exo and KF-exo are consistent with an analogous proof-reading function for the WRN-exo domain, with its relatively weak activity being stimulated by Ku70/80 during certain DNA metabolism functions such as DNA end-joining. Therefore, similar to the results provided by the nuclease-polymerase structures in understanding mechanisms underlying high fidelity DNA synthesis, these structural, mutational and biochemical analyses may help to provide a basis for a more detailed molecular understanding of WRN-specific functions in genomic maintenance including its roles in the reduction of cancer and aging phenotypes.

Methods

WRN-exo domain identification and protein purification.

A WRN-exo construct, amino acids 1-333, was cloned into a pET28b vector (Novagen) that appends an N-terminal hexa-His tag. WRN_{1-333} was over expressed in *E. coli* BL21 (DE3) PLysS cells (Novagen) by IPTG induction. Cells were resuspended in Tris-HCl buffer, pH 7.5 and the protein was affinity purified from sonicated cell lysate by a Ni-NTA agarose resin column (Qiagen). Two further column chromatography steps, using (G.E. Health Care) Superdex 200 gel filtration column, with 500mM NaCl and a MonoQ ion exchange chromatography column, 50mM to 1M NaCl gradient, purified the protein to near homogeneity. Limited proteolysis was conducted on WRN_{1-333} combined with N-terminal sequencing and tandem mass spectroscopy (MS/MS), to define the domain boundaries of the minimal WRN-exo. From these methods, a minimal WRN_{38-236} exonuclease construct was cloned, expressed and purified using the same protocol. For crystallographic phasing studies selenomethionine (SeMet) derivatized $WRN_{38-236,}$ protein was expressed by using *E. coli* B834 DE3 PLysS cells (Novagen) grown in selenomethionine containing media, and the protein was purified as above. Mutagenesis was performed with the QuickChange Site-Directed Mutagenesis Kit (Stratagene) to construct the WRN-exo mutants, E84A, L88A, V114I, T172P, W145A, and Y212F. The mutant proteins were purified by the same protocol as for the wild type protein. Recombinant full-length human Ku70/80 heterodimer was purified from Sf9 insect cells infected with recombinant baculovirus harboring the hKu70 and hKu80 cDNAs[16].

Crystallization, Data Collection and Analysis

Initial crystallization conditions were discovered for WRN_{38-236} construct by combining our crystallization experiments with the robotic crystallization screens of Syrrx, Inc. Further screening efforts optimized crystallization conditions, which consisted of 5μl of 4.5mg/ml WRN_{38-236} protein solution, buffered in 25mM Tris HCl, 100mM NaCl, pH7.5, mixed with 5μl 1% MPEG 2K, 200mM Na Acetate, pH 4.5 from the reservoir solution and 1μl EDTA additive. Crystals were grown by vapor diffusion, in sitting drop trays incubated at $4^{o}C$. Flash-frozen single crystals, supplemented with 20% ethylene glycol cryoprotectant in the mother liquor, were used for X-ray diffraction data collection at $100^{o}K$. Data sets were collected to 2.0 Å on a Q210 ADSC CCD detector at beamline 5.0.2 of the Advanced Light Source, Lawrence Berkeley National Laboratory. Crystallographic data processing, phasing and refinement details are described in the supplementary methods. A Ramachandran plot of the refined WRN-exo structural model shows 92.6% of the residues in the most favored region and the remaining 7.4% in the additionally allowed region. To define WRN-exo metal ion chelation, WRN_{38-236} crystals were first washed with mother liquor to remove EDTA. The crystals were then incubated with mother liquor and 50 mM Mn acetate, Mg acetate or Europium chloride (Hampton Research) for at least 12 hrs before data collection. Phases were obtained by molecular replacement from the native apo-structure, and model building is described in the supplementary methods. The crystallographic data collection, processing, refinement statistics for the native, selenomethione and metal ion soaked crystals are summarized in Table 1.

Exonuclease Activity Assay

Exonuclease activity assays were carried out under conditions reported previously[16], with a 35-bp double-stranded DNA oligonucleotide with 5-nucleotide single-strand extensions on both 5′-termini, (5′-GGC GCA AAT CAA CAC GTT GAC TAC CGT CTT GAG GCA GAG T) (5′-CCG GGA CTC TGC CTC AAG ACG GTA GTC AAC GTG TTG ATT T). The oligonucleotide was 5′-end labeled on a single strand with [γ-^{32}P]-ATP using T4 polynucleotide kinase (New England Biolabs). 20 fmol of probe was incubated for 30-60 min at 37 °C with 20-200 pmol (as noted) of WRN-exo, in 50 mM HEPES (pH 7.5), 50 mM KCl, 1mM DTT and 5 mM metal ion cofactor, either $MgCl_2$, $MnCl_2$ or $EuCl_2$, or 2.5 mM of each in mixed reactions, as noted. Reactions of full-length WRN when compared to the minimal exonuclease domain used the same 35 base pair substrate and reaction conditions. The reactions were incubated with 5 mM $MnCl_2$ cofactor and 1.25 pmol of full-length WRN protein (WRN) or 8.3 pmoles WRN-exo. The Ku70/80 exonuclease stimulation assay used the same substrate and buffer conditions with 5 mM Mg^{2+} cofactor, and reactions were incubated 60 min. This assay was conducted under simiiar conditions (enzyme excess) as studies on full length WRN-Ku interaction[19-24]. Nuclease reactions with increasing amounts of purified Ku70/80 (0, 0.1, 0.5, 2, and 5.3 pmoles) and 20 fmol of DNA substrate (as above) were incubated at 37°C for 60 min with 80 pmol WRN-exo, 3.7 pmol KF-exo, or 0.25 pmol ExoIII). Reaction products from these assays were resolved on 16 % PAGE-TBE gels containing 8.3 M urea.

Microhomology Search Assay

We adapted a previously reported assay[38] for our DNA end-joining analysis. Cell lines used for the assay were fibroblasts from a WS individual (73-26) and from a normal individual (82-6), and Chinese hamster ovary wild type AA8 and V3 (DNA-PKcs $^{-/-}$) controls. Patient 73-26 is a Japanese female and carries a homozygous mutation, IVS25–1G3C, which causes skipping of exon 26 followed by a frameshift. Cells were infected with a pBABE retrovirus carrying the catalytic component of human telomerase (hTERT) and a puromycin resistance gene, selected, and expanded as described[16]. Cultures infected with virus lacking insert senesced 10 (73-26) and 40 (82-6) doublings after infection, whereas cultures infected with pBABE-hTERT continued to proliferate for >150 doublings. SV-40 transformed WT (AG07217A) and WS (AG11395) cells were purchased from Coriell Institute. Telomerase-expressing cells (73-26 hTERT and 82-6 hTERT) were then superinfected with an LXSN retrovirus carrying the full length WRN cDNA, and a neomycin resistant gene. Infected cells were selected and expanded as described[16]. The differing WRN cDNAs were wild type, E84A, E84A-K557A and K557A mutants. The WS cells, WS cells complemented with WRN cDNA (73-26 hTERT) and (82-6 hTERT) were grown in Dulbecco's modified Eagle's medium supplemented with 10% fetal calf serum, 4 mM glutamine, and penicillin/streptomycin. Cells were grown in 100 mm dishes to 80% confluency and transfected with 5 μg of linear DNA substrate (pDVG94/pDVG94-XcmI), previously linearized with EcoRV and AfeI enzymes, resulting in formation of blunt ends. The substrate contained either six or ten base pairs of homologous sequence proximal to the termini,. It was transfected into cells using Transfast (Promega) transfection reagent, following the manufacturer's protocol. The

joined DNA substrate was recovered from the cells 48 hours after transfection using Wizard Minipreps Kit (Promega). The recovered plasmid DNA was PCR amplified for 25 cycles across the original break, with the forward (5′-TGCTTCCGGCTCGTATGTTGGTTGGAAT-3′) and reverse (5′-CTCCATTTTAGCTTCCTTAGCTCCTG-3′) primers in the presence of ^{32}P-dCTP. PCR products were purified using Sephadex G-25 spin columns (Qiagen) and 50% of the sample was digested with BstXI/XcmI restriction enzyme at 55/37^{o}C for 4 hrs and resolved by 8% PAGE, visualized by phosphor imaging, and quantified using Image Quant software. The data presented are two independently run sets of experiments. For the western blot, cells were harvested, washed three times in ice cold PBS and sonicated in 1X SDS-sample buffer (50 mM Tris-HCl pH 6.8, 2% SDS, 10% glycerol and 100 mM DTT). 30 μg of protein was separated on 10% SDS-PAGE, transferred to nitrocellulose membrane, probed with WRN polyclonal antibody raised against N-terminal domain of hWRN, Ku70 goat polyclonal antibody (SC1486, Santa Cruz) and Ku80 (SC9034, Santa Cruz), and the signal was detected using ECL reagent (Amersham).

Coordinates: The coordinates have been deposited in the Protein Data Bank as 2FBT for native WRN-exo, 2FBY, Eu^{3+} complex, 2FBV, Mn^{2+} complex, 2FBX, Mg^{2+} complex and 2FC0, Mn^{2+}-dGMP complex.

Acknowledgements

We thank Judith Campisi and Shurong Huang for the full-length WRN clone and WRN cell lines used in the microhomology repair assay, David King for MS/MS analysis of

proteolytic digests, and Duncan McRee and Syrrx Inc for use of the Syrrx Inc robotic crystallization screens to discover initial WRN-exo crystallization conditions. We thank Scott Williams and Julie Tubbs for critical reading of the manuscript. This work was supported by NIH grants CA104660 (JAT, SMY), CA63503 (PKC) and CA92584 (JAT, PKC, DJC).

Abbreviations

WS, Werner syndrome; WRN, Werner syndrome protein; WRN-exo, Werner syndrome protein 3′-5′ exonuclease domain; DSB, double-strand break; DNA-PK, DNA-dependent protein kinase; KF, Klenow fragment; KF-exo, *E. coli* DNA PolI Klenow fragment 3′-5′ proofreading exonuclease domain, dGMP, 2′-deoxyguanosine 5′-monophosphate.

Fig. 1. WRN-exo active site struture and experimental electron density. Wall-eyed stereodiagram of WRN-exo residues 81-86, which include the conserved active site residues D82 and E84. Initial phasing for the WRN-exo crystal structure was gained from MAD phasing of a selenomethione derived WRN-exo dataset. These initial phases were used to determine the WRN-exo structure to an increased 2.0 Å resolution. The depicted 2.0 Å 2FoFc electron density map is contoured at 1,3 & 5 σ in blue, magenta and red, respectively.

Fig. 2. WRN-exo fold, structure, and active site structural chemisry. (a) WRN-exo α–β fold with α-helices 1-7 (blue), β-strands 0-7 (green), and loops (gray). The conserved active site residues (yellow tubes with red oxygen spheres) chelate the two manganese ions (magenta). (b) Structural superimposition of the WRN-exo (blue) and the Klenow fragment exonuclease (yellow) showing that the cores and most secondary structural elements are conserved with the most notable alterations in the WRN β2-β3 and α6-α7 loop regions. Metal ions at sites M_A and M_B (blue, WRN-exo; orange, Klenow fragment exonuclease) are also similarly positioned. (c) Structural superimposition of the WRN-exo (blue), and the *A. thaliana* protein homolog (cyan; 1VK0.pdb) showing that the core secondary structural elements and β2-β3 loop are conserved between the two structures. The WRN β0-β7 sheet is disrupted in the *A. thaliana* homolog, instead β0 stacks against the central sheet and α6 is in the approximate position of WRN β7. Positions of the *A. thaliana* β0 and α6 are marked. (d) Superimposition of WRN-exo, KF-exo and the *A. thaliana* homolog active sites. WRN-exo (blue) and KF-exo residues (yellow) are strictly conserved. In the *A. thaliana* homolog (cyan), a Y54 replaces WRN E84, A188 replaces Y212 and an E192 replaces D216. (e) Structure-based sequence alignment of WRN-exo with KF-exo and *A. thaliana* homolog. Identical residues (red) and well-conserved residues (blue), which cluster in the active site region, with conserved active site residues in WRN-exo and KF-exo (red star) supporting similar 3′-5′ nuclease activities. Secondary structural elements (WRN-exo blue, KF-exo yellow, and *A. thaliana* homolog cyan) include helices, strands, 3_{10} helices marked as η.

Fig. 3. WRN-exo metal ion dependence and structural analyses. (a) WRN-exo metal ion dependent nuclease activity assay. Reactions contained 50 pmol of WRN-exo and 20 fmol of 5′-labeled 35 base-pair DNA substrate with 5-base 5′-overhanging termini. 5 mM divalent cation(s) were added as noted in each lane, except in lane 1 control, and the reactions were incubated at 37°C for 30 min. WRN-exo 3′-5′ dsDNA nuclease activity is supported by Mg^{2+} or Mn^{2+} ions but not by Eu^{2+} or in the absence of divalent cations. Addition of Eu^{2+} inhibits nuclease activity in the presence of equimolar Mg^{2+} or Mn^{2+} ions. The DNA digestion pattern with equimolar Mg^{2+} and Mn^{2+} is indistinguishable from that of Mn^{2+} alone. (b) Two Mn^{2+} ions, purple, are chelated in the WRN active site in the absence of DNA, metal ion bonds with distances are depicted by dashed magenta lines. The inner metal ion, M_A, is directly coordinated by D82, E84, D216 and the outer metal ion, M_B, directly ligates one side chain D82 that bridges the two metal ions. D143 has an indirect interaction with the M_B metal ion via two water molecules. (c) The WRN active site also accommodated two of the larger lanthanide Eu^{3+} ions (blue) in the absence of substrate (metal ion bonds as dashed blue lines). (d) Overlay of WRN Mn^{2+} and Eu^{3+} metal ion complex structures, coloring scheme as in (b) and (c). Incorporation of Eu^{3+} metal ions at sites M_A and M_B does not cause significant alterations to the WRN active site.

Fig. 4. WRN-exo DNA binding cleft. (a) The electrostatic surface of WRN-exo, with 3 bases modeled from the Klenow fragment exonuclease structure, pdb code 1KFS.pdb. DNA substrate is well accommodated into the WRN DNA binding surface, which is significantly more positively charged when compared with (b), the KF-exo electrostatic surface diagram. The KF-exo molecule is in the same orientation as the WRN-exo, with the 3 bases observed bound in the active site. Color bar: red, -2.0 kT/e to blue, + 2.0 kT/e (c) Active sites and substrate binding regions of WRN in green and KF-exo in blue. The conserved WRN Y212 has flipped out from the active site and the conserved L88, in the β2-β3 loop, has moved 10 Å from the KF-exo equivalent, L361. (d) The WRN-exo active site with a ssDNA model from KF-exo structure, showing that residues potentially binding the terminal nucleotide include R196, C197 and W85. (e) Structure-based alignment of the β2-β3 substrate binding loop region of human WRN residues 80-106 and homologous WRN sequences. Y89 and K93 are strictly conserved and N90, R91 well conserved among the sequences, implicating roles for substrate binding.

Fig. 5. Nuclease activities of WRN, WRN-exo, and WRN-exo point mutants, and nuclease modulation by Ku70/80. (a) Nuclease activity of WRN-exo and WRN-exo point mutants on a 5′-labeled 35 base pair substrate with 5-base 5′-overhanging termini. Increasing amounts (8, 25, and 80 pmoles) of the wild type protein (WT) or point mutants were incubated with ~20 fmol 5′-labeled DNA and Mn^{2+} cofactor at 37° C for 60 min, and resolved on denaturing acrylamide gels. Triangles denote increasing nuclease concentration steps, and "S" indicates the control reaction without WRN-exo. (b) Nuclease reactions with increasing amounts of purified Ku70/80 (0, 0.1, 0.5, 2, and 5.3 pmol) and ~20 fmol of DNA substrate (as above) were incubated at 37°C for 60 min with Mg^{2+} cofactor and resolved on denaturing acrylamide gels. Ku70/80/DNA ratios are equivalent in each nuclease series. To visualize reaction products for all three nucleases under identical reaction conditions, nuclease concentrations were set according to the respective nuclease specific activity (80 pmol WRN-exo, 3.7 pmol KF-exo, and 0.25 pmol ExoIII). For comparing WRN and WRN-exo (far right), the nuclease reactions were as above but with Mn^{2+} cofactor and included either no nuclease (S), 1.25 pmol full-length WRN protein (WRN), or 8.3 pmol WRN-exo.

Fig. 6. Nuclease and helicase activity act together based upon an in vivo plasmid end-joining assay. (a) A schematic representation of the plasmid-rejoining assay. Linear plasmid is transfected into cells then recovered after 48 hours. Rejoined plasmid is PCR amplified across the junction, then analyzed by BstXI restriction. Microhomology-mediated end-joining generates a BstXI restriction site. (b) Reporter plasmids having 6 base pairs of microhomology at the termini were recovered from wild type (AA8) or DNA-PKcs defective (V3) Chinese hamster ovary cells, PCR amplified (denoted, PCR), and restricted with BstXI (where indicated), generating two restriction fragments (RF1 and RF2). (c) Assay as above, conducted with wild type (WT) or Werner syndrome (WS) human fibroblasts, or with WS cells complemented with WRN cDNA (WS-c) or WRN cDNA harboring a nuclease inactivating mutation (E84A). (d) End-joining assay with a reporter plasmid containing 10 base-pairs of terminal microhomology, performed with WS human fibroblasts complemented by expression of wild type (WS-c), nuclease inactivated (E84A), both nuclease and helicase inactivated (E84A-K577A), or helicase inactivated (K577A) WRN cDNAs. (e) Western blot of cellular extracts of the assayed cell lines, probed for WRN and Ku80 to normalize loading.

Fig. 7. WRN-exo Hexameric Ring Model, dGMP binding site, and altered processing for the W145A mutant. (a) The WRN ring homology model, with individually colored WRN-exo subunits was built by structural superimposition to the *A. thaliana* homolog, pdb code 1VK0.pdb. The active site of the exonuclease (grey metal ion spheres) faces the center of the ring. The central cavity diameter of the WRN ring (about 30 Å in diameter by 35 Å deep) is large enough to accommodate dsDNA, and similar to that observed in Ku70/80[49]. (b) DNA processing is altered in a WRN-exo Trp145A mutant. Control reactions with DNA alone or with 10 pmol of Ku70/80 are indicated. WRN-exo and W145A reactions contained 20 fmol of radiolabeled dsDNA substrate, approximately 200 pmol of each WRN nuclease variant, and an increasing amount of Ku70/80 (0.06, 0.6 and 6 pmol), denoted by triangles. (c) Fo-Fc electron density map of WRN-exo dGMP soak (3σ blue, 5σ red). dGMP stacks against Trp145, consistent with this region interacting with DNA substrate at the center of the ring. (d) The similar internal and external dimensions of the WRN-exo hexamer model (right) and Ku70/80 bound to DNA (left) suggest a possible interaction mode, which would place the protruding β2-β3 loop (left face) adjacent to the Ku dimer, and/or allow Ku to provide a suitable DNA orientation.

References

1. Goto, M. Hierarchical deterioration of body systems in Werner's syndrome: implications for normal ageing. *Mechanisms of Ageing & Development* **98**, 239-54 (1997).
2. Opresko, P.L., Cheng, W.H., von Kobbe, C., Harrigan, J.A. & Bohr, V.A. Werner syndrome and the function of the Werner protein; what they can teach us about the molecular aging process. *Carcinogenesis* **24**, 791-802 (2003).
3. Yu, C.E. et al. Positional cloning of the Werner's syndrome gene. *Science* **272**, 258-62 (1996).
4. von Kobbe, C. & Bohr, V.A. A nucleolar targeting sequence in the Werner syndrome protein resides within residues 949-1092. *J Cell Sci* **115**, 3901-7 (2002).
5. Matsumoto, T., Shimamoto, A., Goto, M. & Furuichi, Y. Impaired nuclear localization of defective DNA helicases in Werner's syndrome. *Nat Genet* **16**, 335-6 (1997).
6. Moser, M.J. et al. WRN helicase expression in Werner syndrome cell lines. *Nucleic Acids Res* **28**, 648-54 (2000).
7. Goto, M. et al. Immunological diagnosis of Werner syndrome by down-regulated and truncated gene products. *Human Genetics* **105**, 301-7 (1999).
8. Hickson, I.D. RecQ helicases: caretakers of the genome. *Nature Reviews. Cancer* **3**, 169-78 (2003).
9. Moser, M.J., Holley, W.R., Chatterjee, A. & Mian, I.S. The proofreading domain of Escherichia coli DNA polymerase I and other DNA and/or RNA exonuclease domains. *Nucleic Acids Res* **25**, 5110-8 (1997).
10. Mushegian, A.R., Bassett, D.E., Jr., Boguski, M.S., Bork, P. & Koonin, E.V. Positionally cloned human disease genes: patterns of evolutionary conservation and functional motifs. *Proc Natl Acad Sci U S A* **94**, 5831-6 (1997).
11. Huang, S. et al. The premature ageing syndrome protein, WRN, is a 3'-->5' exonuclease. *Nat Genet* **20**, 114-6 (1998).
12. von Kobbe, C., Thoma, N.H., Czyzewski, B.K., Pavletich, N.P. & Bohr, V.A. Werner syndrome protein contains three structure-specific DNA binding domains. *J Biol Chem* **278**, 52997-3006 (2003).
13. Opresko, P.L., Laine, J.P., Brosh, R.M., Jr., Seidman, M.M. & Bohr, V.A. Coordinate action of the helicase and 3' to 5' exonuclease of Werner syndrome protein. *Journal of Biological Chemistry* **276**, 44677-87 (2001).
14. Comai, L. & Li, B. The Werner syndrome protein at the crossroads of DNA repair and apoptosis. *Mech Ageing Dev* **125**, 521-8 (2004).
15. Cheng, W.H. et al. Linkage between Werner syndrome protein and the Mre11 complex via Nbs1. *J Biol Chem* **279**, 21169-76 (2004).
16. Yannone, S.M. et al. Werner syndrome protein is regulated and phosphorylated by DNA-dependent protein kinase. *J Biol Chem* **276**, 38242-8 (2001).
17. Baynton, K. et al. WRN interacts physically and functionally with the recombination mediator protein RAD52. *J Biol Chem* **278**, 36476-86 (2003).

18. Sakamoto, S. et al. Werner helicase relocates into nuclear foci in response to DNA damaging agents and co-localizes with RPA and Rad51. *Genes Cells* **6**, 421-30 (2001).
19. Cooper, M.P. et al. Ku complex interacts with and stimulates the Werner protein. *Genes Dev* **14**, 907-12 (2000).
20. Li, B. & Comai, L. Functional interaction between Ku and the werner syndrome protein in DNA end processing. *J Biol Chem* **275**, 39800 (2000).
21. Orren, D.K. et al. A functional interaction of Ku with Werner exonuclease facilitates digestion of damaged DNA. *Nucleic Acids Res* **29**, 1926-34 (2001).
22. Li, B. & Comai, L. Requirements for the nucleolytic processing of DNA ends by the Werner syndrome protein-Ku70/80 complex. *J Biol Chem* **276**, 9896-902 (2001).
23. Li, B. & Comai, L. Displacement of DNA-PKcs from DNA ends by the Werner syndrome protein. *Nucleic Acids Res* **30**, 3653-61 (2002).
24. Karmakar, P. et al. Werner protein is a target of DNA-dependent protein kinase in vivo and in vitro, and its catalytic activities are regulated by phosphorylation. *J Biol Chem* **277**, 18291-302 (2002).
25. Li, B., Navarro, S., Kasahara, N. & Comai, L. Identification and biochemical characterization of a Werner's syndrome protein complex with Ku70/80 and poly(ADP-ribose) polymerase-1. *J Biol Chem* **279**, 13659-67 (2004).
26. Beese, L.S. & Steitz, T.A. Structural basis for the 3'-5' exonuclease activity of Escherichia coli DNA polymerase I: a two metal ion mechanism. *Embo J* **10**, 25-33 (1991).
27. Bruns, C.M., Hubatsch, I., Ridderstrom, M., Mannervik, B. & Tainer, J.A. Human glutathione transferase A4-4 crystal structures and mutagenesis reveal the basis of high catalytic efficiency with toxic lipid peroxidation products. *Journal of Molecular Biology* **288**, 427-39 (1999).
28. Brautigam, C.A., Aschheim, K. & Steitz, T.A. Structural elucidation of the binding and inhibitory properties of lanthanide (III) ions at the 3'-5' exonucleolytic active site of the Klenow fragment. *Chem Biol* **6**, 901-8 (1999).
29. Brautigam, C.A. & Steitz, T.A. Structural principles for the inhibition of the 3'-5' exonuclease activity of Escherichia coli DNA polymerase I by phosphorothioates. *Journal of Molecular Biology* **277**, 363-77 (1998).
30. Wang, J., Yu, P., Lin, T.C., Konigsberg, W.H. & Steitz, T.A. Crystal structures of an NH2-terminal fragment of T4 DNA polymerase and its complexes with single-stranded DNA and with divalent metal ions. *Biochemistry* **35**, 8110-9 (1996).
31. Doublie, S., Tabor, S., Long, A.M., Richardson, C.C. & Ellenberger, T. Crystal structure of a bacteriophage T7 DNA replication complex at 2.2 A resolution.[see comment]. *Nature* **391**, 251-8 (1998).
32. Hopfner, K.P. et al. Crystal structure of a thermostable type B DNA polymerase from Thermococcus gorgonarius. *Proceedings of the National Academy of Sciences of the United States of America* **96**, 3600-5 (1999).
33. Kamath-Loeb, A.S., Welcsh, P., Waite, M., Adman, E.T. & Loeb, L.A. The enzymatic activities of the Werner syndrome protein are disabled by the amino acid polymorphism R834C. *Journal of Biological Chemistry* **279**, 55499-505 (2004).

34. Bernstein, D.A., Zittel, M.C. & Keck, J.L. High-resolution structure of the E.coli RecQ helicase catalytic core. *EMBO Journal* **22**, 4910-21 (2003).
35. Oshima, J., Huang, S., Pae, C., Campisi, J. & Schiestl, R.H. Lack of WRN results in extensive deletion at nonhomologous joining ends. *Cancer Research* **62**, 547-51 (2002).
36. Crabbe, L., Verdun, R.E., Haggblom, C.I. & Karlseder, J. Defective telomere lagging strand synthesis in cells lacking WRN helicase activity. *Science* **306**, 1951-3 (2004).
37. Laud, P.R. et al. Elevated telomere-telomere recombination in WRN-deficient, telomere dysfunctional cells promotes escape from senescence and engagement of the ALT pathway. *Genes Dev* **19**, 2560-70 (2005).
38. Melek, M., Gellert, M. & van Gent, D.C. Rejoining of DNA by the RAG1 and RAG2 proteins. *Science* **280**, 301-3 (1998).
39. Verkaik, N.S. et al. Different types of V(D)J recombination and end-joining defects in DNA double-strand break repair mutant mammalian cells. *European Journal of Immunology* **32**, 701-9 (2002).
40. Tauchi, H. et al. Nbs1 is essential for DNA repair by homologous recombination in higher vertebrate cells. *Nature* **420**, 93-8 (2002).
41. Chen, L. et al. WRN, the protein deficient in Werner syndrome, plays a critical structural role in optimizing DNA repair. *Aging Cell* **2**, 191-9 (2003).
42. Lan, L. et al. Accumulation of Werner protein at DNA double-strand breaks in human cells. *J Cell Sci* (2005).
43. Monnat, R.J., Jr. & Saintigny, Y. Werner syndrome protein--unwinding function to explain disease. *Sci Aging Knowledge Environ* **2004**, re3 (2004).
44. Swanson, C., Saintigny, Y., Emond, M.J. & Monnat, R.J., Jr. The Werner syndrome protein has separable recombination and survival functions. *DNA Repair (Amst)* **3**, 475-82 (2004).
45. Doublie, S., Sawaya, M.R. & Ellenberger, T. An open and closed case for all polymerases. *Structure* **7**, R31-5 (1999).
46. Huang, S. et al. Characterization of the human and mouse WRN 3'-->5' exonuclease. *Nucleic Acids Res* **28**, 2396-405 (2000).
47. Karow, J.K., Newman, R.H., Freemont, P.S. & Hickson, I.D. Oligomeric ring structure of the Bloom's syndrome helicase. *Curr Biol* **9**, 597-600 (1999).
48. Xue, Y. et al. A minimal exonuclease domain of WRN forms a hexamer on DNA and possesses both 3'- 5' exonuclease and 5'-protruding strand endonuclease activities. *Biochemistry* **41**, 2901-12 (2002).
49. Walker, J.R., Corpina, R.A. & Goldberg, J. Structure of the Ku heterodimer bound to DNA and its implications for double-strand break repair. *Nature* **412**, 607-14 (2001).
50. Shin, D.S., Chahwan, C., Huffman, J.L. & Tainer, J.A. Structure and function of the double-strand break repair machinery. *DNA Repair (Amst)* **3**, 863-73 (2004).

Figure 1.

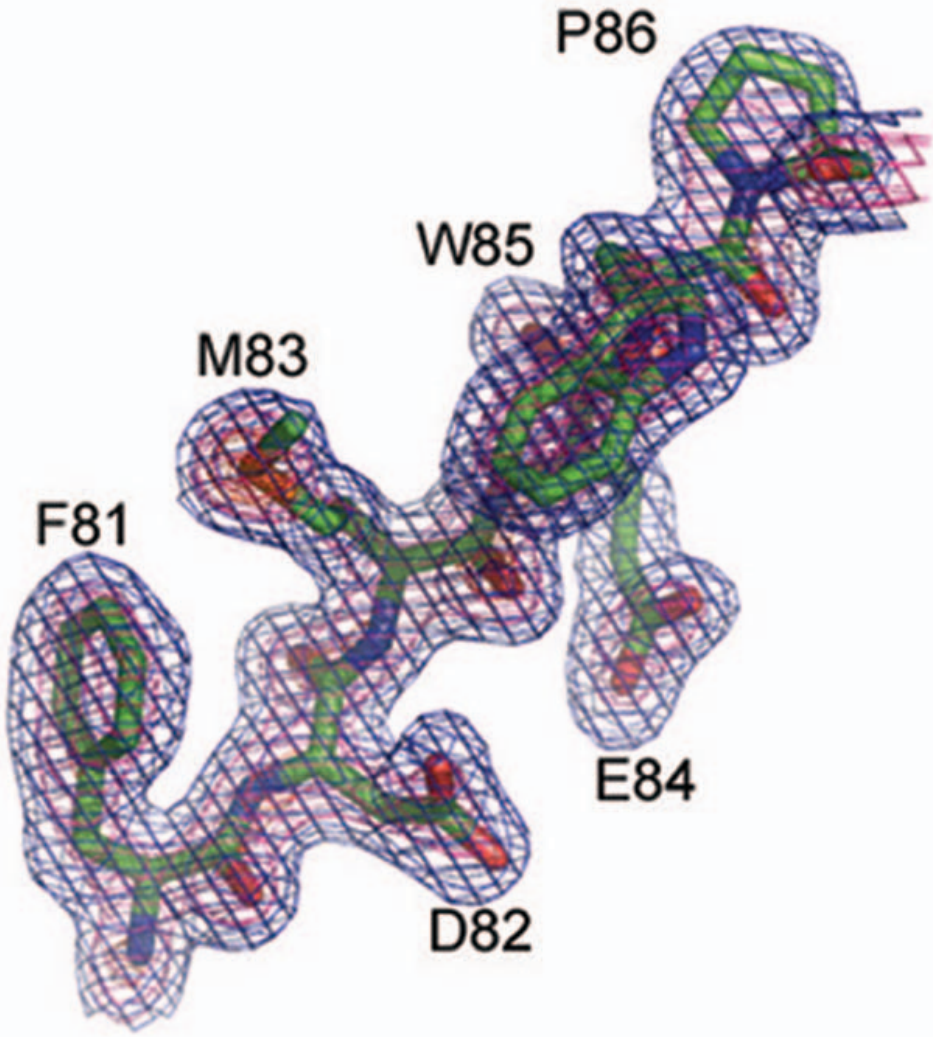

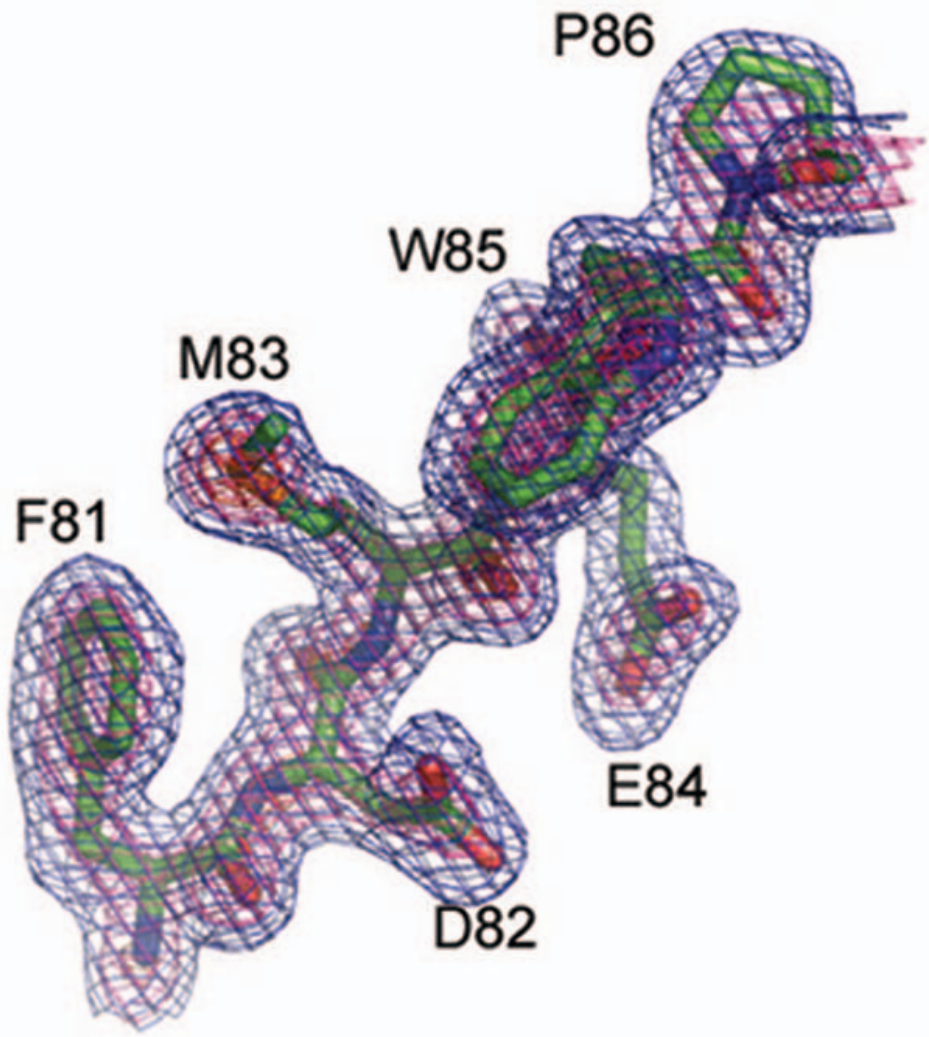

Figure 2.

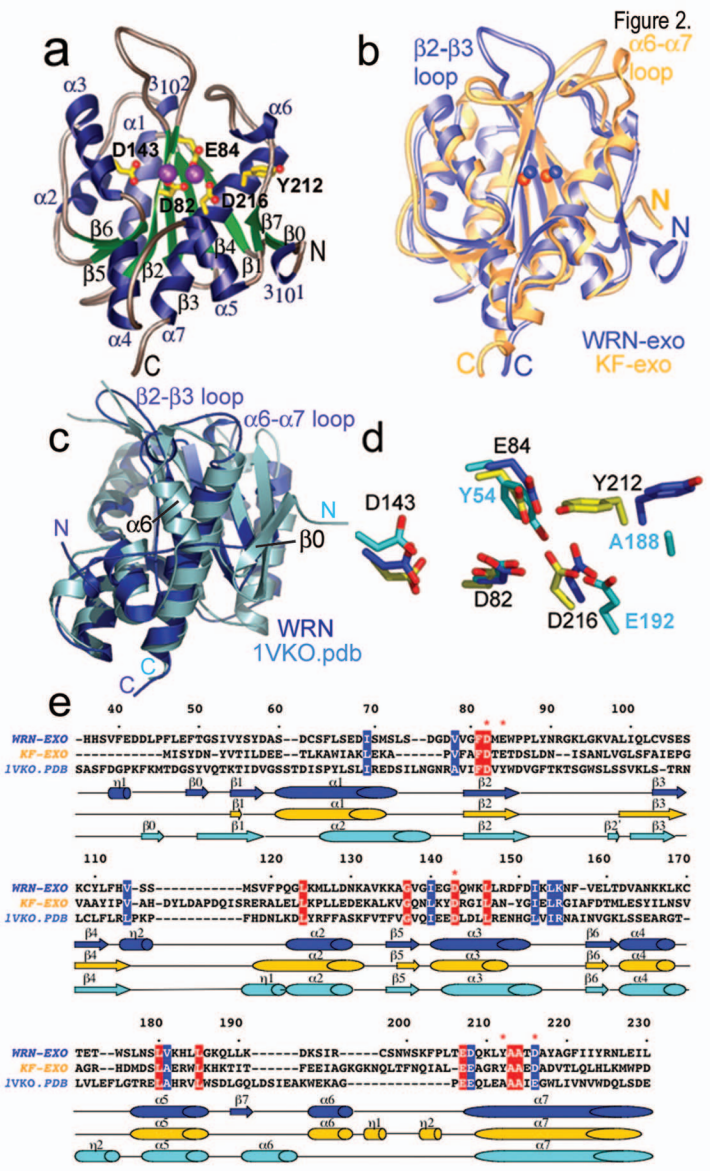
a
α3
310 2
α1
α6
D143
E84
Y212
α2
D82
D216
β6
β7
β0
N
β4
β5
β2
β1
β3
α5
310 1
α4
α7
C
b
β2-β3 loop
α6-α7 loop
N
N
WRN-exo
KF-exo
C
C
c
β2-β3 loop
α6-α7 loop
N
N
α6
β0
WRN
1VKO.pdb
C
C
d
E84
D143
Y54
Y212
A188
D82
D216
E192
e
WRN-EXO -HHSVFEDDLPFLEFTGSIVYSYDAS--DCSFLSEDISMSLS--DGDVVGFDMEWPPLYNRGKLGKVALIQLCVSES
KF-EXO ----------MISYDN-YVTILDEE--TLKAWIAKLEKA------PVFAFDTETDSLDN--ISANLVGLSFAIEPG
1VKO.PDB SASFDGPKFKMTDGSYVQTKTIDVGSSTDISPYLSLIREDSILNGNRAVIFDVYWDVGFTKTSGWSLSSVKLS-TRN
WRN-EXO KCYLFHV-SS----------MSVFPQGFKMLLDNKAVKKAVGIEGFQWKFLRDFDIKLKNF-VELTDVANKKLKC
KF-EXO VAAYIPV-AH-DYLDAPDQISRERALELFKPLLEDEKALKVFQNGKYDRGIIAN-YGHELRGIAFDTMLESYILNSV
1VKO.PDB LCLFLRLPKP----------FHDNLKDIYRFFASKFVTFVSQHEEDILDLLRENHGEVIRNAINVGKLSSEARGT-
WRN-EXO TET--WSLNSLVKHLFGKQLLK------DKSIR-----CSNWSKFPLTEDQKLYAATDAYAGFIIYRNLEIL
KF-EXO AGR--HDMDSLAERWLKHKTIT------FEEIAGKGKNQLTFNQIALLEEAGRYAAEDADVTLQLHLKMWPD
1VKO.PDB LVLEFLGTREFAHRVDWSDLGQLDSIEAKWEKAG----------PFEQLEAAIEEGWLIVNVWDQLSDE

Figure 3.

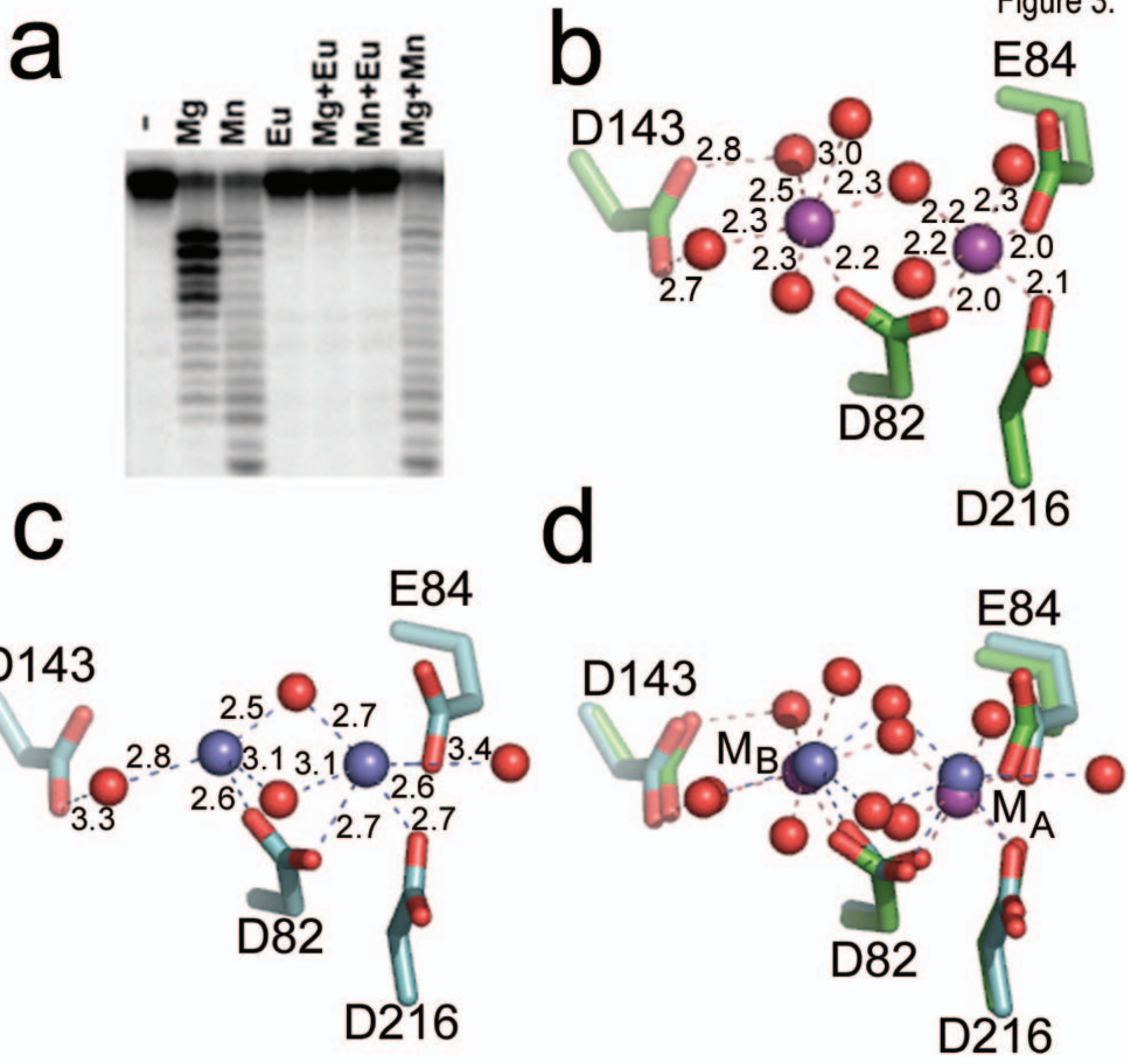
a
-
Mg
Mn
Eu
Mg+Eu
Mn+Eu
Mg+Mn
b
E84
D143
2.8
3.0
2.5
2.3
2.3
2.3
2.2
2.3
2.2
2.2
2.0
2.3
2.0
2.1
2.7
D82
D216
c
E84
D143
2.5
2.7
2.8
3.1
3.1
3.4
2.6
2.6
3.3
2.7
2.7
D82
D216
d
E84
D143
M_B
M_A
D82
D216

Figure 4.

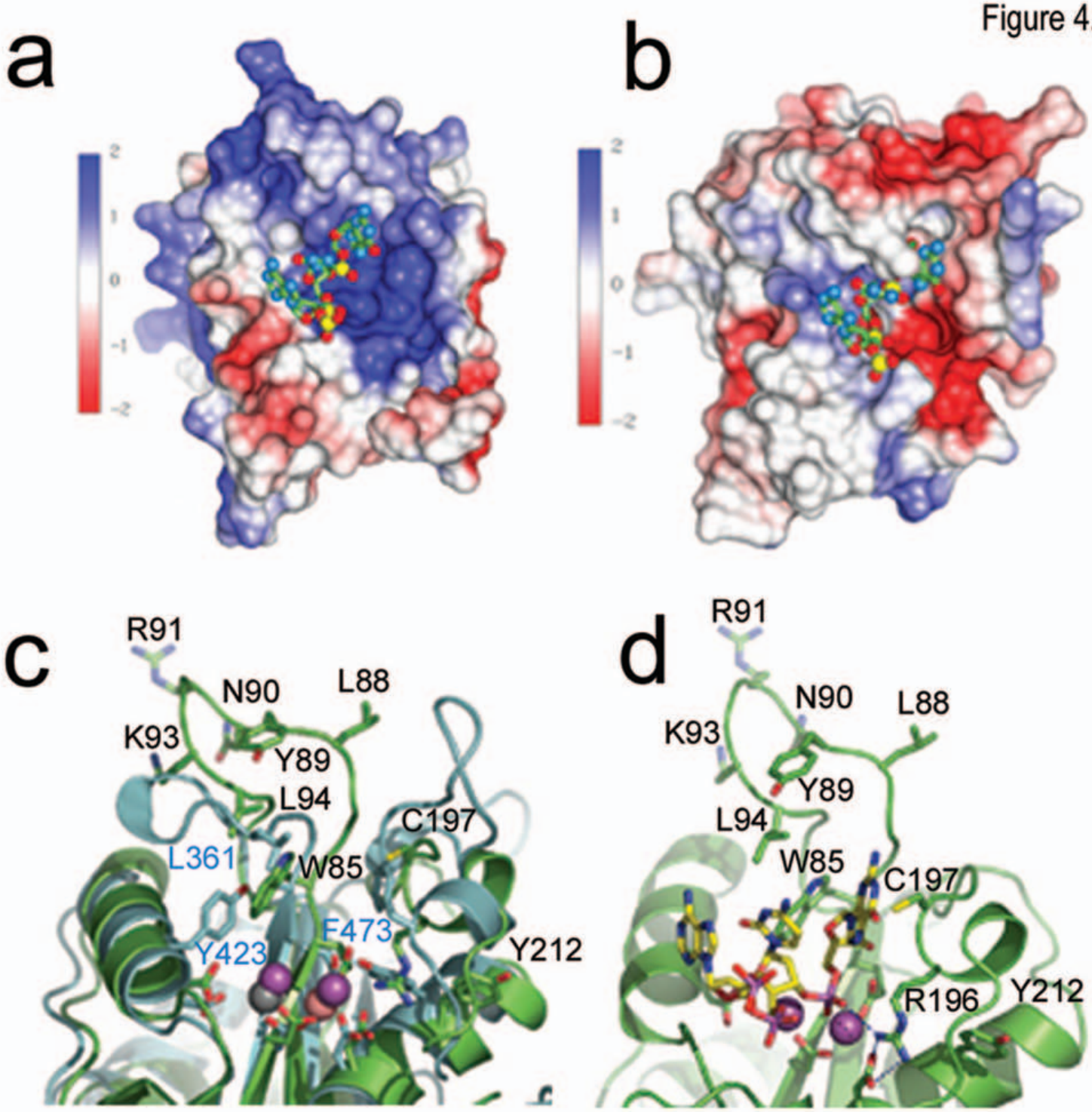

e

```
WRN H. sapiens          GFDMEWPPLYNRGKLGKVALIQLCVSE
WRN P. pygmaeus         GFDMEWPPLYKKRKLGKVALIQLCVSE
WRN P. troglodytes      GFDMEWPPLYNRGKLGKVALIQLCVSE
WRN M. musculus         GFDMEWPPIYKPGKRSRVAVIQLCVSE
WRN C. familiaris       GFDMEWPPVYTKRKPSRVALIQLCVSE
WRN X. laevis           GFDIEWPPVYTKGKTGKVALIQVCVSE
                        ***:****:*. .* .:**:*******
```

Figure 5.

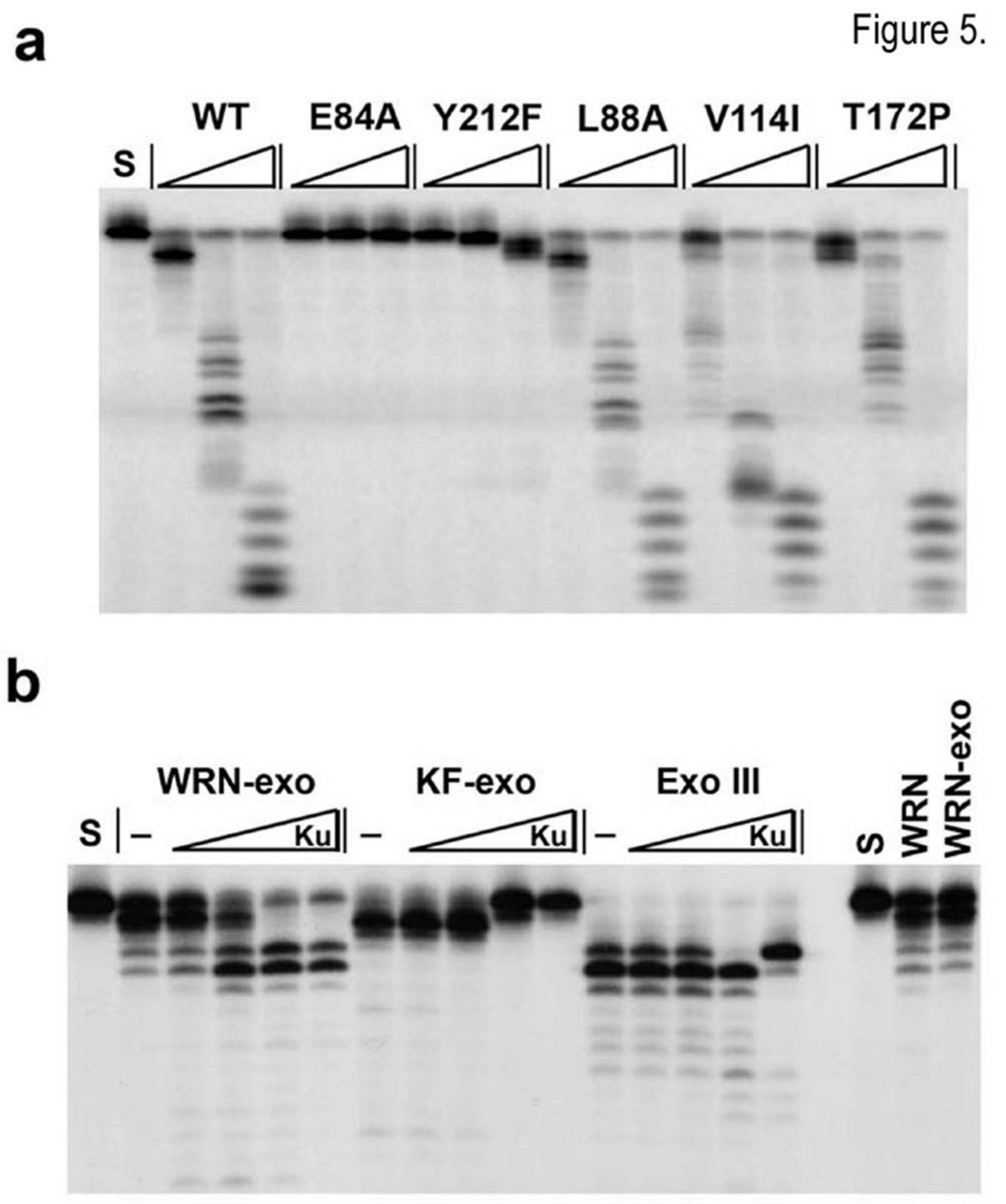
a
WT
E84A
Y212F
L88A
V114I
T172P
S
b
WRN-exo
KF-exo
Exo III
S
–
Ku
–
Ku
–
Ku
S
WRN
WRN-exo

Figure 6.

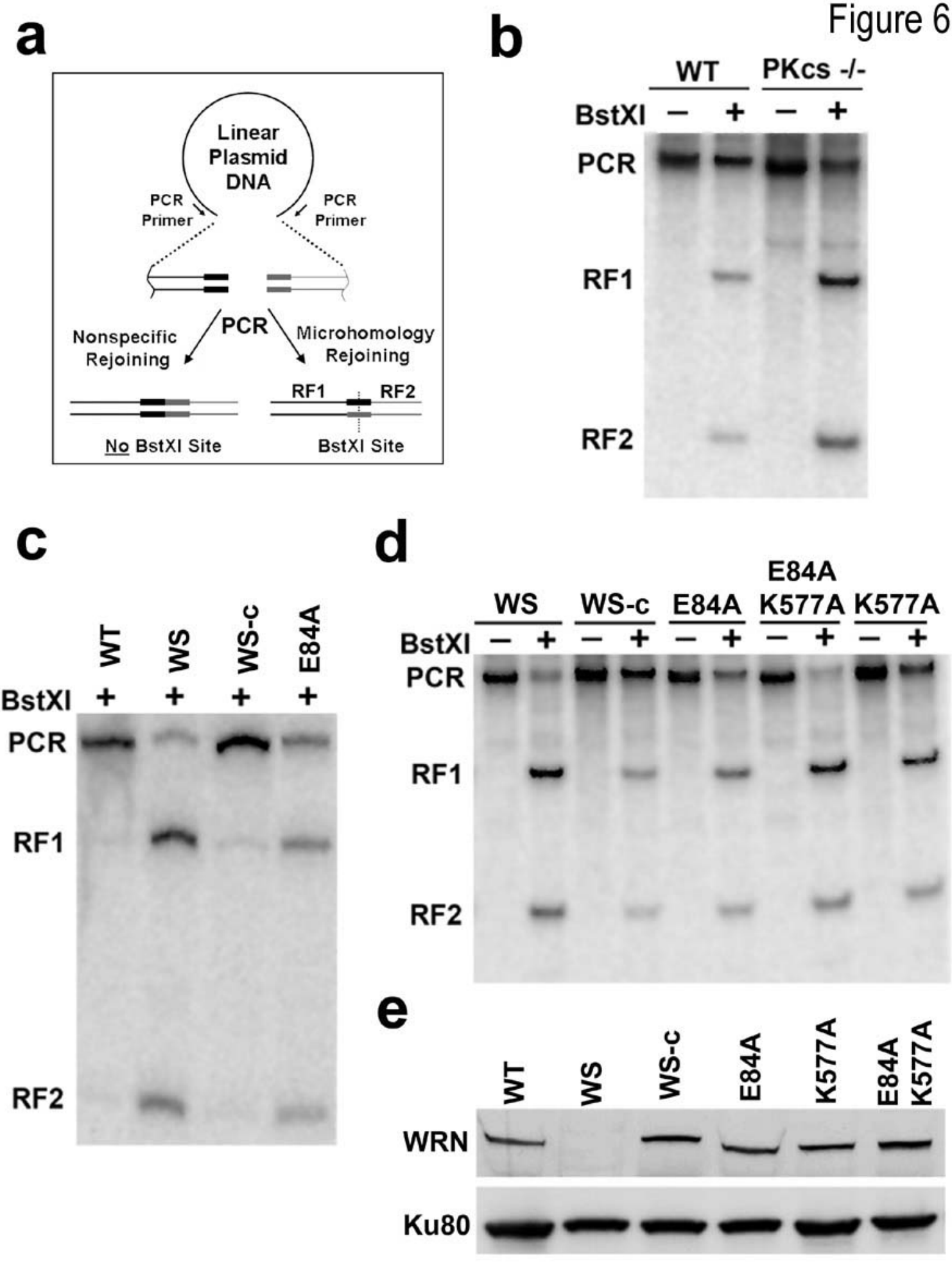
a
Linear Plasmid DNA
PCR Primer
PCR Primer
PCR
Nonspecific Rejoining
Microhomology Rejoining
RF1
RF2
No BstXI Site
BstXI Site
b
WT
PKcs -/-
BstXI
PCR
RF1
RF2
c
WT
WS
WS-c
E84A
BstXI
PCR
RF1
RF2
d
WS
WS-c
E84A
E84A K577A
K577A
BstXI
PCR
RF1
RF2
e
WT
WS
WS-c
E84A
K577A
E84A K577A
WRN
Ku80

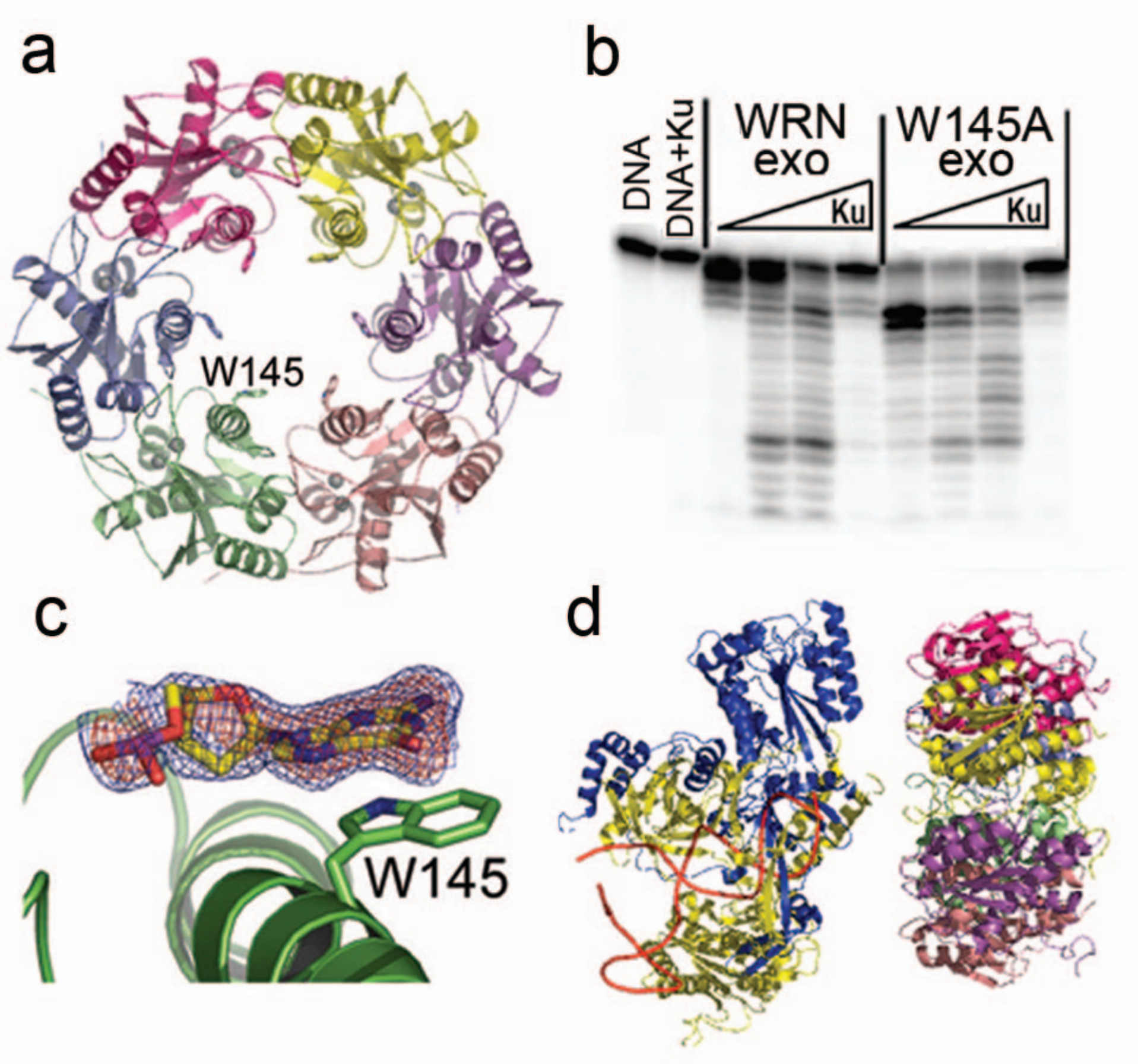
a
W145
b
DNA
DNA+Ku
WRN exo
Ku
W145A exo
Ku
c
W145
d

Table1. Crystallographic Data and Refinement Statistics.

							SeMet	
Dataset	**Native**	**Mg^{2+}**	**Mn^{2+}**	**Eu^{3+}**	**dGMP**	**peak**	**edge**	**remote**
Wavelength, Å	**1.0**	**0.92**	**0.92**	**0.95**	**0.95**	**0.9793**	**0.9794**	**0.9636**
Resolution, Å	**27.9 – 2.05**	**19.7 – 2.2**	**19.8 – 2.4**	**27.8 – 2.0**	**38.9 - 2.0**	**20 – 2.5**	**20 – 2.5**	**20 – 2.5**
Theoretical/ observed reflections	**22,265 21,308 (2,999)**	**18,422 17,851 (2,487)**	**14,255/ 13,337 (1,891)**	**23,787 22, 764 (3,221)**	**24,473 24,008 (3,601)**	**23,101 22,639 (2,305)**	**23,127 21,763 (2,218)**	**23,227 21,834 (2,114)**
% Completeness	**95.7 (86.8%)**	**96.9 (87.1)**	**93.7 (85.6)**	**95.7 (87.1)**	**98.1 (93.4)**	**98.0 (99.1)**	**94.1 (95.7)**	**94.0 (95.1)**
$\langle I/\sigma I \rangle$	**20.8 (3.0)**	**29.7 (5.7)**	**18.7 (3.8)**	**39.4 (3.4)**	**54.2 (8.5)**	**14.5 (2.9)**	**13.2 (2.5)**	**11.1 (1.8)**
R_{merge}	**7.5 (33.1)**	**5.6 (36.5)**	**7.5 (34.9)**	**5.6 (34.9)**	**7.5 (32.1)**	**8.5 (37.8)**	**9.2 (28.7)**	**9.3 (33.9)**
Wilson B	**14.6**	**25.8**	**14.8**	**22.8**	**20.6**			
Model statistics								
R_{free}	**24.1**	**26.2**	**27.7**	**24.5**	**23.8**			
R_{work}	**20.1**	**24.2**	**23.7**	**22.1**	**22.3**			
Rmsd dev. bond length, angle	**.006 1.1**	**.006 1.2**	**.006 1.2**	**.005 1.2**	**.005 1.2**			

Single crystals were used for each data set collected and data for the highest resolution shell is shown in brackets.